

Forecasting with time series imaging

Xixi Li^a, Yanfei Kang^a, Feng Li^{b,*}

^a*School of Economics and Management, Beihang University, Beijing 100191, China.*

^b*School of Statistics and Mathematics, Central University of Finance and Economics, Beijing 100081, China.*

Abstract

Feature-based time series representations have attracted substantial attention in a wide range of time series analysis methods. Recently, the use of time series features for forecast model averaging has been an emerging research focus in the forecasting community. Nonetheless, most of the existing approaches depend on the manual choice of an appropriate set of features. Exploiting machine learning methods to automatically extract features from time series becomes crucially important in state-of-the-art time series analysis. In this paper, we introduce an automated approach to extract time series features based on images. Time series images are first transformed into recurrence images, from which local features can be extracted using computer vision algorithms. The extracted features are used for forecast model averaging. Our experiments show that forecasting based on automatically extracted features, with less human intervention and a more comprehensive view of the raw time series data yields comparable performances with the best methods proposed in the largest forecasting competition dataset (M4).

Keywords: Forecasting, Time series feature extraction, Recurrence plots, Forecast combination.

1. Introduction

Time series *features* are a collection of statistical representations of time series characteristics. Feature-based time series representation has attracted remarkable attention in a vast majority of time series data mining tasks. Most of the time series problems, including time series clustering (e.g., Wang et al., 2006; Bandara et al., 2020), classification (e.g., Fulcher and Jones, 2014; Nanopoulos et al., 2001) and anomaly detection (e.g., Hyndman et al., 2015; Tala-gala et al., 2019), are eventually attributed to the quantification of similarity among time series

*Corresponding author

Email addresses: lixixi199407@buaa.edu.cn (Xixi Li), yanfeikang@buaa.edu.cn (Yanfei Kang), feng.li@cufe.edu.cn (Feng Li)

URL: <https://orcid.org/0000-0001-8769-6650> (Yanfei Kang), <https://orcid.org/0000-0002-4248-9778> (Feng Li)

data using time series feature representations. [Fulcher \(2018\)](#) presents a comprehensive range of features that can be used to represent a time series, such as global features, subsequence features and other hybrid features, for classifying time series ([Fulcher and Jones, 2014](#)), labeling the emotional content of speech ([Fulcher et al., 2013](#)), etc. Specifically, in time series forecasting, instead of the typical time series forecasting procedure – fitting a model to the historical data and simulating future data based on the fitted model – selecting the most appropriate forecasting model or averaging a number of candidate models based on time series features have been popular alternative approaches developed in the last few decades (e.g., [Adam, 1973](#); [Collopy and Armstrong, 1992](#); [Wang et al., 2009](#); [Petropoulos et al., 2014](#); [Kang et al., 2017](#)).

Many attempts have been made on feature-based model selection and averaging procedures for univariate time series forecasting. For example, [Collopy and Armstrong \(1992\)](#) provided 99 rules using 18 features to combine four extrapolation methods by examining a rule base to forecast annual economic and demographic time series; [Arinze \(1994\)](#) described the use of an artificial intelligence technique to improve the forecasting accuracy, build an induction tree to model time series features and develop the most accurate forecasting method; [Shah \(1997\)](#) constructed several individual selection rules for forecasting using discriminant analysis based on 26 time series features; [Meade \(2000\)](#) used 25 summary statistics of time series as explanatory variables in predicting the relative performances of nine forecasting methods based on a set of simulated time series with known properties; [Petropoulos et al. \(2014\)](#) proposed “horses for courses” and measured the effects of seven time series features on the forecasting performances of 14 popular forecasting methods on the monthly data in the M3 dataset ([Makridakis and Hibon, 2000](#)); more recently, [Kang et al. \(2017\)](#) visualized the performances of different forecasting methods in a two-dimensional principal component feature space and provided a preliminary understanding of their relative performances. [Talagala et al. \(2018\)](#) presented a general framework for forecast model selection using meta-learning. They use random forest to select the best forecasting method based on time series features. [Montero-Manso et al. \(2020\)](#) trained a meta-model to obtain the weights of various forecasting methods and made a weighted forecasting combination. The input of the meta-model is a set of features calculated on the training data, while the output is a group of weights assigned to each candidate forecasting method. Their method ranked 2nd in the M4 Competition ([Makridakis et al., 2018](#)).

Having revisited the literature on feature-based time series forecasting, we found that (i) although researcher often highlight the usefulness of time series features in selecting the best forecasting method, most of the existing approaches depend on the manual choice of an appropriate set of features, which makes the forecast process rely on the data and the expertise of

the forecasters (Fulcher, 2018) and inflexible, and (ii) the current literature on feature-based forecasting focuses on global features of time series, leaving local characteristics underemphasized. In some instances, the local dynamics of time series contain important information such as a heart failure in medical signals or an irregular weather change. Therefore, exploiting automated feature extraction from time series data becomes vital. Inspired by the recent work of Hatami et al. (2017) and Wang and Oates (2015), this paper aims to explore time series forecasting based on model averaging with the idea of time series imaging, from which time series global and local features can be automatically extracted using computer vision algorithms. The proposed approach enables automated feature extraction. This new approach for time series forecasting is more flexible than forecasting based on manually curated time series features.

The rest of the paper is organized as follows. Section 2 presents our feature extraction method for time series imaging. In Section 3, we describe how to assign weights to a group of candidate forecasting methods based on time series images features and perform forecasting method combinations based on those weights. Section 4 applies our image-based time series forecasting combination method to the M4 dataset. Section 5 concludes the paper and discusses ways forward.

2. Feature extraction from time series imaging

In this paper, we extract time series features based on time series imaging in two steps. In the first step, we encode the time series into images using recurrence plots. In the second step, time series features are extracted from images using image processing techniques. We consider two different approaches for image feature extraction: spatial bag-of-features (SBoF) model and convolutional neural networks (CNNs). We describe the details in the following sections.

2.1. Encoding time series to images

We use recurrence plots (RPs) to encode time series data into images, which provide a way to visualize the periodic nature of a trajectory through a phase space (Eckmann et al., 1987) and are able to contain all relevant dynamical information in the time series (Thiel et al., 2004). A recurrence plot of time series x , showing when the time series revisits a previous state, can be formulated as

$$R(i, j) = \Theta(\epsilon - \|x_i - x_j\|),$$

where $R(i, j)$ is the element of the recurrence matrix R ; i indexes time on the x-axis of the recurrence plot, j indexes time on the y-axis. ϵ is a predefined threshold, and $\Theta(\cdot)$ is the Heaviside step function. In short, one draws a black dot when x_i and x_j are closer than ϵ .

Instead of binary output, an unthresholded RP is not binary and is difficult to quantify. We use the following modified RP, which balances the binary output and unthresholded RP.

$$R(i, j) = \begin{cases} \epsilon & \|x_i - x_j\| > \epsilon, \\ \|x_i - x_j\| & \text{otherwise,} \end{cases}$$

which gives more values than a binary RP and results in colored plots. Fig. 1 shows three typical examples of recurrence plots. They reveal different patterns of recurrence plots for time series with randomness, periodicity, chaos and trend. We can see that the recurrence plots shown in the right column well depict the predefined patterns in the time series shown in the left column.

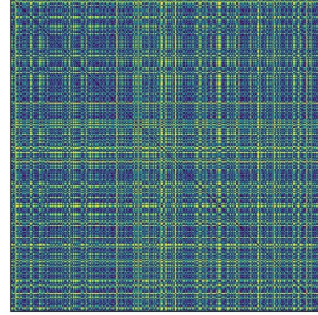
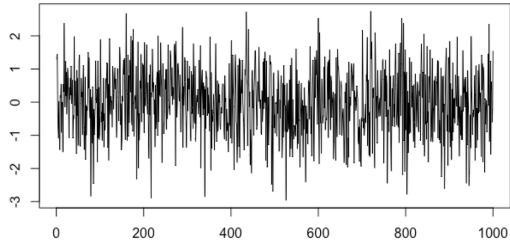
2.2. Feature extraction with the spatial bag-of-features (SBoF) model

Fig. 2 shows the framework of our method for image-based time series feature extraction using the SBoF model. It consists of three steps: (i) detect key points with the scale-invariant feature transform (SIFT) algorithm (Lowe, 1999) and find basic descriptors with k -means; (ii) generate the representation based on the locality constrained linear coding (LLC) method (Wang et al., 2010); and (iii) extract spatial information via spatial pyramid matching (SPM) and pooling. We interpret the details in each step, respectively.

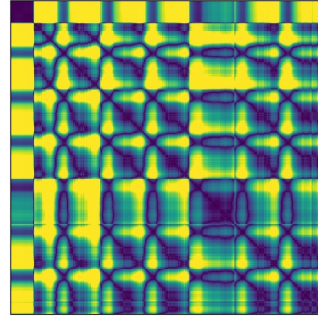
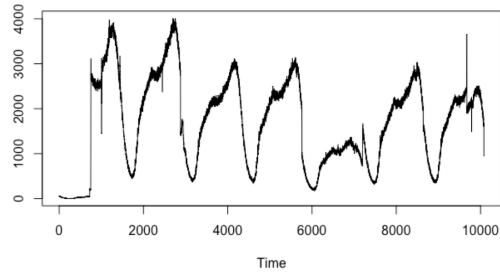
The original bag-of-features (BoF) model, which extracts features from one-dimensional signal segments, has achieved great success in time series classification (Baydogan et al., 2013; Wang et al., 2013). Hatami et al. (2017) transformed a time series into two-dimensional recurrence images with a recurrence plot (Eckmann et al., 1987) and then applied the BoF model. Extracting time series features is then equivalent to identifying key points in images, which are called key descriptors. A promising algorithm is the SIFT algorithm (Lowe, 1999), which is used to detect and describe local features in images by identifying the maxima/minima of the difference of Gaussians (DoG) that occur at the multiscale spaces of an image as its key descriptors. It consists of the following four steps.

1. **Detect extreme values in the scale spaces.** We search over all the scale spaces and use the Gaussian differential method to identify the potential interest points and select those invariant to scale and orientation.
2. **Find the key points.** The position scale is determined by fitting a model at each candidate position, and the key points are selected according to their stability.
3. **Assign feature directions.** This step assigns the key points one or more directions based on the local gradient direction of the image. To allow for invariance in the features,

Uncorrelated stochastic data(white noise)



Time series with periodicity and chaotic data



Time series with periodicity and trend

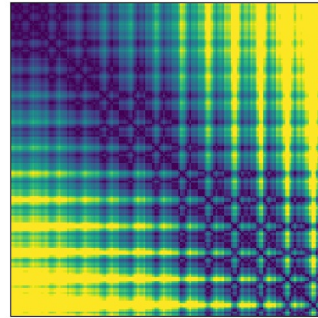
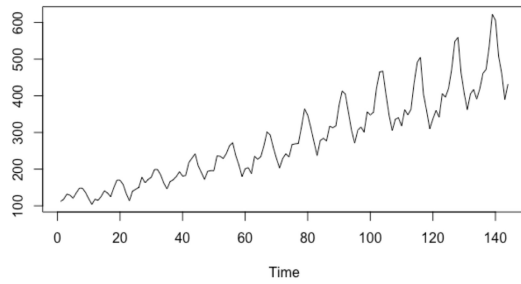


Fig. 1: Typical examples of recurrence plots (right column) for time series data with different patterns (left column): uncorrelated stochastic data, i.e., white noise (top), a time series with periodicity and chaos (middle), and a time series with periodicity and trend (bottom).

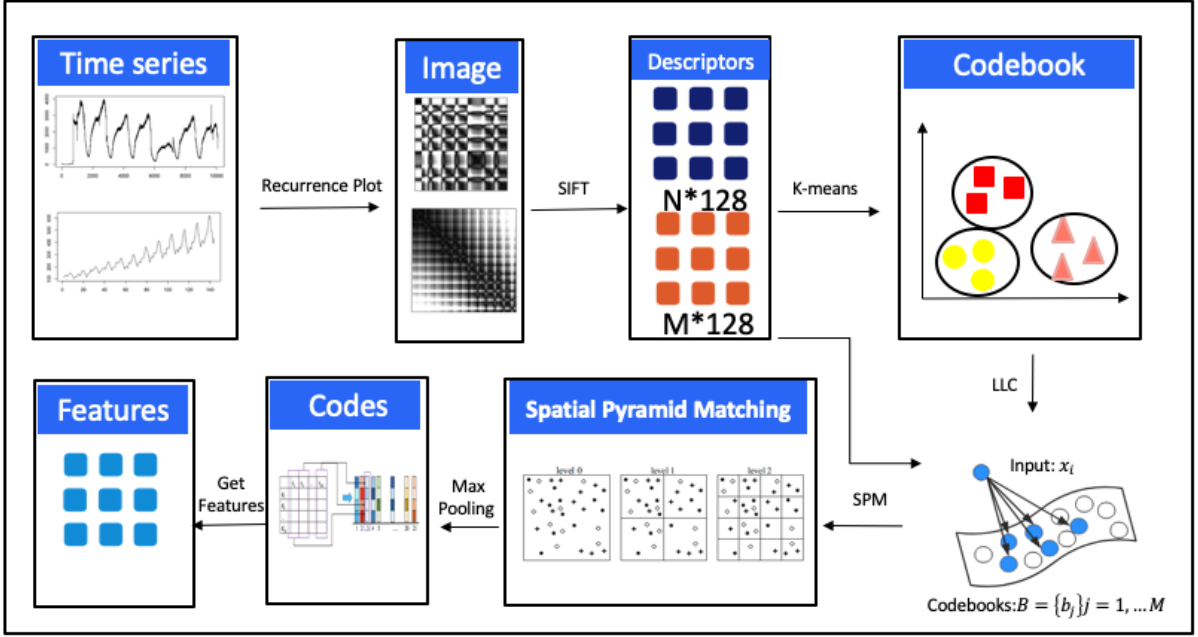


Fig. 2: Image-based time series feature extraction with spatial bag-of-features model. It consists of four steps: (i) encode a time series as an image with recurrence plots; (ii) detect key points with SIFT and obtain the basic descriptors with k -means for the codebook; (iii) generate the representation based on LLC; and (iv) extract spatial information via SPM and max pooling.

all subsequent operations are about how to transform the direction, scale and position of the key points.

4. **Describe key points.** Within the neighborhood around each feature point, the local gradient of the image is measured at selected scales, which is transformed into a representation that allows larger local shape deformations and illumination transformations. The SIFT method uses a 128-dimensional vector to characterize the key descriptors in an image. First, an 8-direction histogram is established in each 4×4 subregion, and a16 subregions in the 16×16 region around the key points are calculated. Then, it calculates the magnitude and direction of each pixel's gradient magnitude and adds to the subregion. In the end, 128-dimensional image data based on histograms are generated.

Each descriptor can be projected onto its local coordinate system, and the projected coordinates are integrated by max pooling to generate the final representation with the LLC method, which utilizes the locality constraints to project each descriptor onto its local coordinate system (Wang et al., 2010). The projected coordinates are integrated by max pooling to generate the

final representation:

$$\min_c \sum_i^N \|x_i - Bc_i\|^2 + \lambda \|d_i \odot c_i\|^2, \text{ s.t. } 1^T c_i = 1, \forall i, \quad (1)$$

where $d_i = \exp(\text{dist}(x_i, B)/\sigma)$ and $x_i \in R^{128 \times 1}$ is the vector of one descriptor. The basic descriptors $B \in R^{128 \times M}$ are obtained by k -means clustering. The representation parameters c_i are used as time series representations through Equation 1. The locality adaptor d_i gives different freedom for each basis vector proportional to its similarity to the input descriptor. We use σ for adjusting the weight decay speed for the locality adaptor, and λ is the adjustment factor. However, in reality, the number of descriptors obtained by the SIFT algorithm is usually very large, which is why Wang et al. (2010) proposed an incremental codebook optimization method for LLC.

The bag-of-features model calculates the distribution characteristics of feature points in the whole image and then generates a global histogram. As a result, the spatial distribution information of the image is lost, and the image may not be accurately identified. To obtain the spatial information of images, we apply a spatial pyramid matching (SPM) method (Lazebnik et al., 2006), which statistically distributes image feature points at different resolutions and has achieved high accuracy on a large dataset of 15 natural scene categories. The image is divided into progressively finer grid sequences at each level of the pyramid, and features are derived from each grid and combined into one large feature vector. Fig. 3 depicts the diagram of the SPM and max pooling process. In this task, we divide the image by 1×1 , 2×2 and 4×4 , and thus obtain 21 subregions. To obtain the representation for each subregion, first we obtain the descriptors for that region. Suppose that we obtain 12 descriptors denoted by $D_i \in R^{12 \times 200}$ for the third region (200 is the dimension of the local linear representation of the descriptor). Then, we can obtain the maximum value of every dimension of D_i . After max pooling, we obtain the feature representation denoted by $f_i \in R^{200 \times 1}$ for the third region. The feature representations of the other twenty regions can be obtained in the same way. Finally, the 21 features are linked together for the final representation of the time series. In this way, the final sizes of the feature vectors are $21 \times 200 = 4200$.

2.3. Feature extraction by fine-tuned deep networks

An alternative to SBoF for image feature extraction is to use a deep CNN, which has achieved great breakthroughs in image processing (Krizhevsky et al., 2012). For example, Berkeley researchers (Donahue et al., 2014) proposed feature extraction methods called DeCAF (a deep convolutional activation feature for generic visual recognition) and directly use deep convolutional neural networks for feature extraction. Their experimental results show that the

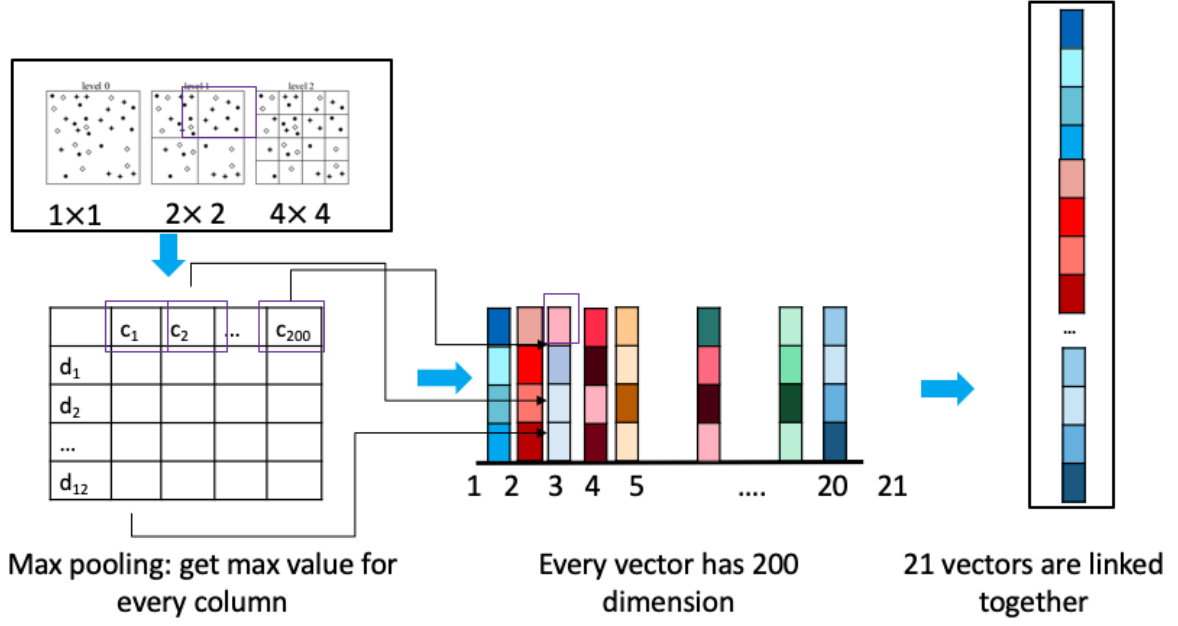


Fig. 3: Spatial pyramid matching and max pooling. The image is divided into progressively finer grid sequences at each level of the pyramid, and features are derived from each grid and combined into one large feature vector. We divide the image by 1×1 , 2×2 and 4×4 , and thus obtain 21 subregions. We first obtain the descriptors for each region. Suppose that we obtain 12 descriptors denoted by $D_i \in R^{12 \times 200}$ for the third region (200 is the dimension of the local linear representation of the descriptor). Then, we can obtain the maximum value of every dimension of D_i . After max pooling, we obtain the feature representation denoted by $f_i \in R^{200 \times 1}$ for the third region. The feature representations of the other 20 regions can be obtained by the same way. Finally, the 21 features are linked together for the final representation for the time series.

feature extraction method has greater advantages in accuracy compared with traditional image features. In addition, some researchers (e.g., [Razavian et al., 2014](#)) use the features acquired by convolutional neural networks as the input of an image classifier, which significantly improves the image classification accuracy.

Nonetheless, the performance of neural networks heavily depends on the setting of the network structure and the hyperparameters. A deeper layer is often essential for achieving higher performance in a task. As a result, extensive computational power is needed. An appealing feature of our time series imaging approach is that there exists a large number of well pretrained neural network models for imaging classification. We could easily transfer the model to our task via transfer learning ([Pan and Qiang, 2010](#)), which has been widely used recently in a variety of fields such as image classification ([Han et al., 2018](#)) and natural language processing ([Ahmad et al., 2020](#)). To simplify our task, we use the fine-tuning approach ([Ge and Yu, 2017](#)) from the field of transfer learning. In short, it uses pretrained networks and makes adjustments to our tasks. We fix the parameters of the previous layers based on the pretrained model with ImageNet data and fine-tune the last few layers for our task. In general, the closer the layer is to the first layer, the more general features can be extracted; the closer the layer is to the back layer, the more specific features for classification tasks can be extracted. In this way, the speed of network training will be greatly accelerated, and it will also greatly improve the performance for our task.

Fig. 4 shows the framework of transfer learning with fine-tuning. In this task, the deep network is trained on the large ImageNet dataset([Deng et al., 2009](#)), and the pretrained network is publicly available. Specifically, we fix the weights of all the previous layers of the pretrained network except for the last fully connected layers and then input our time series images. Finally, the high-dimensional features of the time series images can be obtained from the pretrained network. We consider the following representative architectures in our experiments: ResNet-v1-101([He et al., 2016](#)), ResNet-v1-50([He et al., 2016](#)), Inception-v1([Szegedy et al., 2015](#)) and VGG-19([Simonyan and Zisserman, 2014](#)). The dimensions of the time series features obtained from the pretrained ResNet-v1-101([He et al., 2016](#)), ResNet-v1-50([He et al., 2016](#)), Inception-v1([Szegedy et al., 2015](#)) and VGG-19([Simonyan and Zisserman, 2014](#)) are 2048, 2048, 1024 and 1000, respectively.

3. Time series forecasting with image features

We aim to find the best forecasting method among a pool of candidate forecasting methods or their best combination. The essence is to link the knowledge of forecasting errors from

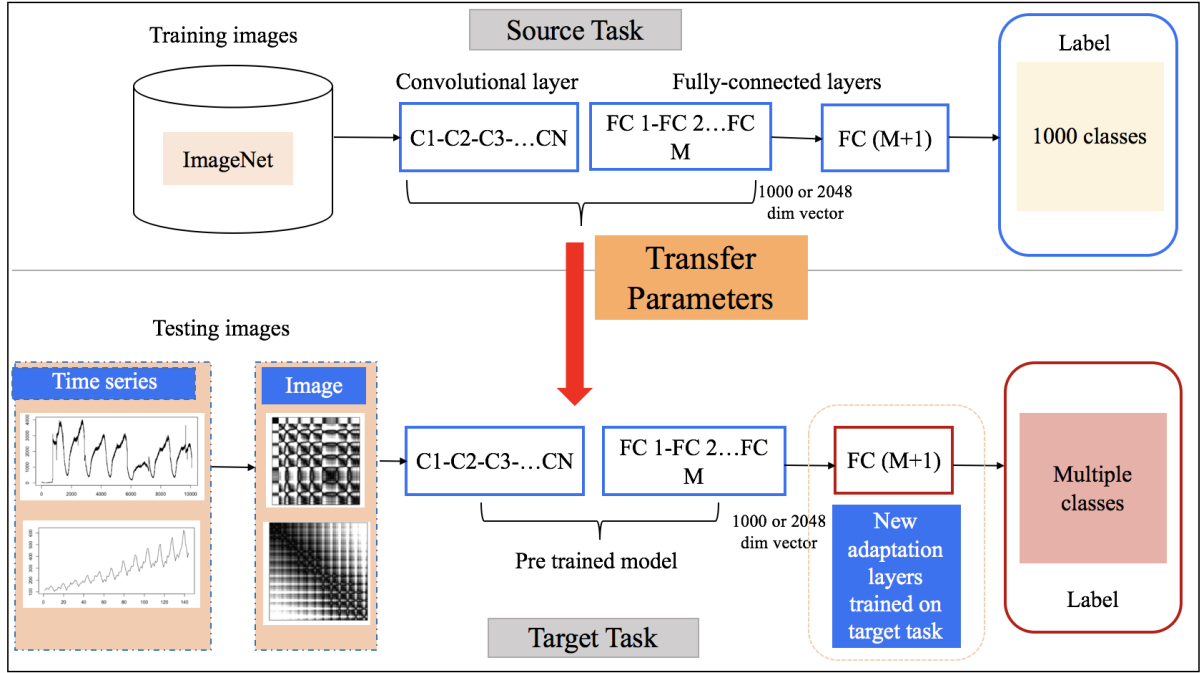


Fig. 4: Framework of transfer learning with fine-tuning. Classic CNN models are trained on a large dataset (ImageNet). For the CNN model, the closer the layer is to the first layer, the more general features can be extracted; the closer the layer is to the back layer, the more specific features for classification tasks can be extracted. To extract time series features, we fix the parameters of all the previous layers except for the last fully connected layer, and fine-tune the last layer for our task. With the trained model, we obtain the final representation of the time series.

different forecasting methods to time series features. Therefore, in this section, we focus on the mapping from the time series image features to forecasting method performances. We use the nine most popular time series forecasting methods as candidates for forecast combination: the automated ARIMA algorithm (ARIMA), automated exponential smoothing algorithm (ETS), NNET-AR model applying a feedforward neural network using autoregressive inputs (NNET-AR), TBATS model (exponential smoothing state space model with a Box-Cox transformation, ARMA errors, trend and seasonal components), seasonal and trend decomposition using LOESS with AR modeling of the seasonally adjusted series (STL-AR), random walk with drift (RW-DRIFT), theta method (THETA), naïve (NAIVE), and seasonal naïve (SNAIVE).

To validate the effectiveness of our image features of the time series, we follow the work of [Montero-Manso et al. \(2020\)](#), who proposed a model-averaging method based on 42 manually curated time series features and won second place in the M4 Competition ([Makridakis et al., 2018](#)), to obtain the weights for forecast combination based on our image features. The overall weighted average (OWA) is used to measure the forecasting accuracies as in the M4 Competition, which is an overall indicator of two accuracy measures, the mean absolute scaled error (MASE) and the symmetric mean absolute percentage error (sMAPE). The individual measures are calculated as follows:

$$\begin{aligned} \text{sMAPE} &= \frac{1}{h} \sum_{t=1}^h \frac{2 |Y_t - \hat{Y}_t|}{|Y_t| + |\hat{Y}_t|}, \\ \text{MASE} &= \frac{1}{h} \frac{\sum_{t=1}^h |Y_t - \hat{Y}_t|}{\frac{1}{n-m} \sum_{t=m+1}^n |Y_t - Y_{t-m}|}, \\ \text{OWA} &= \frac{1}{2} (\text{sMAPE}/\text{sMPAE}_{\text{Naive2}} + \text{MASE}/\text{MASE}_{\text{Naive2}}), \end{aligned}$$

where Y_t is the real value of the time series at point t , \hat{Y}_t is the point forecast, h is the forecasting horizon and m is the frequency of the data (e.g., 4 for quarterly series), and Naïve2 is equivalent to the naïve (NAIVE) method applied to a time series adjusted for seasonal factors.

Our framework for model averaging is shown in Fig. 5. It consists of two parts. In the training process, based on the extracted image features and the OWA values of the nine forecasting methods, we train a feature-based gradient tree boosting model, XGBoost ([Chen and Guestrin, 2016](#)), to produce nine weights for forecast model averaging by minimizing the OWA for the combination of methods. Let f_n be the image features extracted from a time series. O_{nm} is the contribution to the OWA error measure of method $m = 1, 2, \dots, M$ for the series x_n . $p(f_n)_m$ is the output of the XGBoost algorithm corresponding to forecasting method m , based on the features extracted from series x_n . The gradient tree boosting approach minimizes the weighted

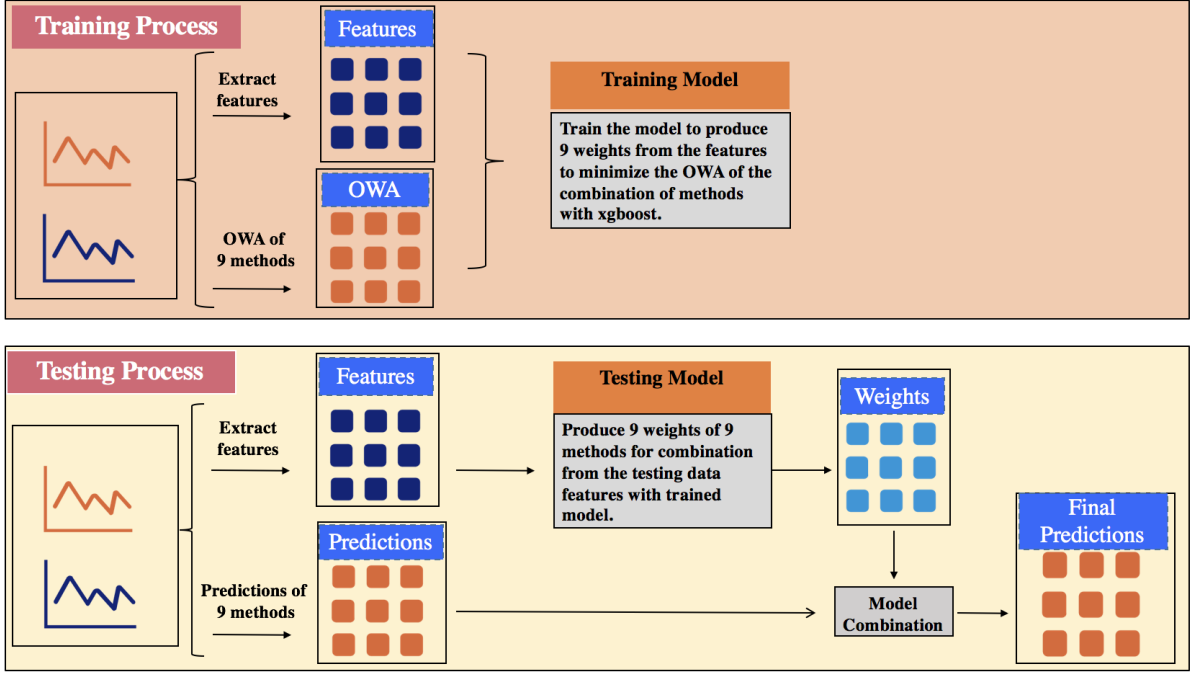


Fig. 5: Framework of forecast model averaging based on automatic feature extraction. In the training process, nine weights are obtained for the forecast model combination using XGBoost. Based on the weights, we obtain the forecasts for the testing data in the testing process.

average loss function as

$$\arg \min_w \sum_{m=1}^M w(f_n)_m O_{nm}.$$

where $w(f_n)_m$ is the softmax-transformed weight for the output $p(f_n)_m$ of the XGBoost model defined as

$$w(f_n)_m = \frac{\exp\{p(f_n)_m\}}{\sum_m \exp\{p(f_n)_m\}}.$$

In the testing process, we use the trained model and the image features extracted from the testing data to obtain the weights of different forecasting models. Finally, based on the weights and forecasts of different models, we can obtain the final forecasts for the testing data.

4. Application to the M4 Competition

4.1. Data

Our application data are from the M4 Competition that consists of 100,000 time series mainly from the economic, finance, demographics and industry domains. In the training process, we divide the original time series in M4 into training and testing periods. The length of the testing period is equal to the forecasting horizon given by the M4 competition. We train an XGBoost model to produce the weights for each candidate forecasting method. In the testing

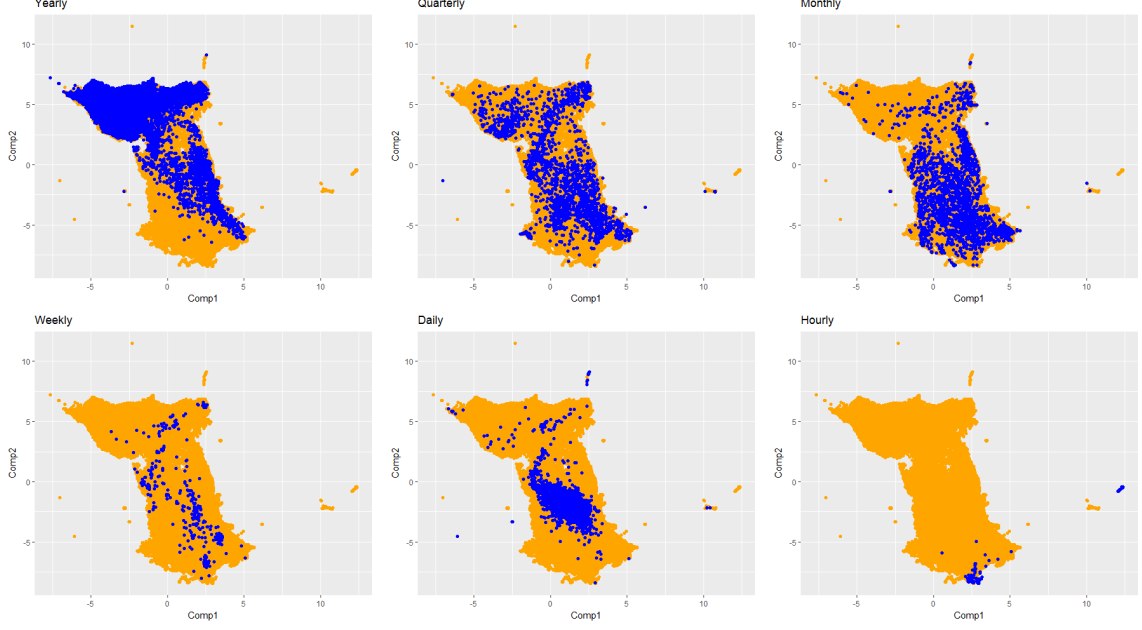


Fig. 6: Two-dimensional feature spaces of the M4 time series with different periods. The blue points highlight areas where the time series with the corresponding seasonal pattern lie.

process, we use the trained model to forecast and evaluate the forecasts based on future M4 data, which were made public after the M4 Competition.

4.2. Forecasting based on automated features

We now apply our method to the M4 data. To illustrate that the extracted image features work, we project the features of the time series with different periods into two-dimensional feature space using t-distributed stochastic neighbor embedding (t-SNE, [Maaten \(2014\)](#)). From Fig. 6, we notice that yearly, quarterly, monthly, daily and hourly data can be well distinguished in the feature spaces, although the features are automatically extracted from time series images.

Following the framework in Fig 5, we obtain the forecasts of M4 based on time series imaging. Our model averaging results are compared with the top ten methods from the M4 Competition. Tables 1, 2 and 3 show the MASE, sMAPE and OWA values for our model-averaging method with the top ten methods from the M4 Competition. Overall, our model averaging method with automated features can achieve comparable performances with the top methods from the M4 Competition. From Table 3, our method ranks sixth overall.

5. Conclusion and future work

Using image features for combining forecast models is proposed by our paper. First, time series are encoded into images. Computer vision algorithms are then applied to extract features from the images, which are used for forecast model averaging. The proposed method enables

Table 1: Model-averaging results compared with the top ten methods from the M4 Competition in terms of the MASE.

Rank	Yearly	Quarterly	Monthly	Weekly	Daily	Hourly	Total
M4 competition							
1	2.980	1.118	0.884	2.356	3.446	0.893	1.536
2	3.060	1.111	0.893	2.108	3.344	0.819	1.551
3	3.130	1.125	0.905	2.158	2.642	0.873	1.547
4	3.126	1.135	0.895	2.350	3.258	0.976	1.571
5	3.046	1.122	0.907	2.368	3.194	1.203	1.554
6	3.082	1.118	0.913	2.133	3.229	1.458	1.565
7	3.038	1.198	0.929	2.947	3.479	1.372	1.595
8	3.009	1.198	0.966	2.601	3.254	2.557	1.601
9	3.262	1.163	0.931	2.302	3.284	0.801	1.627
10	3.185	1.164	0.943	2.488	3.232	1.049	1.614
SIFT	3.135	1.125	0.908	2.266	3.463	0.849	1.579
CNN							
<i>Inception – v1 + XGBoost</i>	3.118	1.121	0.942	2.387	3.344	0.861	1.592
<i>ResNet – v1 – 101 + XGBoost</i>	3.113	1.122	0.919	2.361	3.348	0.845	1.581
<i>ResNet – v1 – 50 + XGBoost</i>	3.111	1.122	0.955	2.375	3.357	0.854	1.598
<i>VGG – 19 + XGBoost</i>	3.153	1.124	0.940	2.332	3.318	0.858	1.599

Table 2: Model-averaging results compared with top ten methods from the M4 Competition in terms of the sMAPE.

Rank	Yearly	Quarterly	Monthly	Weekly	Daily	Hourly	Total
M4 competition							
1	13.176	9.679	12.126	7.817	3.170	9.328	11.374
2	13.528	9.733	12.639	7.625	3.097	11.506	11.720
3	13.943	9.796	12.747	6.919	2.452	9.611	11.845
4	13.712	9.809	12.487	6.814	3.037	9.934	11.695
5	13.673	9.816	12.737	8.627	2.985	15.563	11.836
6	13.669	9.800	12.888	6.726	2.995	13.167	11.897
7	13.679	10.378	12.839	7.818	3.222	13.466	12.020
8	13.366	10.155	13.002	9.148	3.041	17.567	11.986
9	13.910	10.000	12.780	6.728	3.053	8.913	11.924
10	13.821	10.093	13.151	8.989	3.026	9.765	12.114
SIFT	13.896	9.863	12.596	7.899	3.063	11.772	11.816
CNN							
<i>Inception – v1 + XGBoost</i>	13.862	9.835	12.616	8.255	3.117	12.173	11.815
<i>ResNet – v1 – 101 + XGBoost</i>	13.890	9.810	12.566	8.341	3.107	11.772	11.790
<i>ResNet – v1 – 50 + XGBoost</i>	13.847	9.840	12.549	8.033	3.113	11.762	11.778
<i>VGG – 19 + XGBoost</i>	13.987	9.838	12.583	8.408	3.077	11.856	11.826

Table 3: Model-averaging results compared with top 10 methods from the M4 competition in terms of the OWA.

Rank	Yearly	Quarterly	Monthly	Weekly	Daily	Hourly	Total
M4 competition							
1	0.778	0.847	0.836	0.851	1.046	0.440	0.821
2	0.799	0.847	0.858	0.796	1.019	0.484	0.838
3	0.820	0.855	0.867	0.766	0.806	0.444	0.841
4	0.813	0.859	0.854	0.795	0.996	0.474	0.842
5	0.802	0.855	0.868	0.897	0.977	0.674	0.843
6	0.806	0.853	0.876	0.751	0.984	0.663	0.848
7	0.801	0.908	0.882	0.957	1.060	0.653	0.860
8	0.788	0.898	0.905	0.968	0.996	1.012	0.861
9	0.836	0.878	0.881	0.782	1.002	0.410	0.865
10	0.824	0.883	0.899	0.939	0.990	0.485	0.869
SIFT	0.820	0.858	0.863	0.839	1.009	0.498	0.848
CNN							
<i>Inception – v1 + XGBoost</i>	0.816	0.856	0.880	0.880	1.022	0.511	0.852
<i>ResNet – v1 – 101 + XGBoost</i>	0.817	0.855	0.868	0.880	1.021	0.497	0.848
<i>ResNet – v1 – 50 + XGBoost</i>	0.815	0.856	0.884	0.866	1.023	0.498	0.852
<i>VGG – 19 + XGBoost</i>	0.825	0.857	0.878	0.878	1.011	0.502	0.854

automated feature extraction, making it more flexible than using manually selected time series features. In addition, our image features are able to depict local features of time series as well as global features. To the best of our knowledge, this is the first paper that applies imaging to time series forecasting. Our experiments show that our method is able to produce comparable forecast accuracies with the top methods from the largest time series competition (M4).

Acknowledgments

Yanfei Kang’s research and Feng Li’s research were supported by the National Natural Science Foundation of China (no. 11701022 and no. 11501587, respectively).

References

References

- Adam, E. E. (1973), ‘Individual item forecasting model evaluation’, *Decision Sciences* **4**(4), 458–470.
- Ahmad, Z., Jindal, R., Ekbal, A. and Bhattacharyya, P. (2020), ‘Borrow from rich cousin: transfer learning for emotion detection using cross lingual embedding’, *Expert Systems with Applications* **139**, 112851.
- Arinze, B. (1994), ‘Selecting appropriate forecasting models using rule induction’, *Omega-international Journal of Management Science* **22**(6), 647–658.
- Bandara, K., Bergmeir, C. and Smyl, S. (2020), ‘Forecasting across time series databases using recurrent neural networks on groups of similar series: a clustering approach’, *Expert Systems With Applications* **140**, 112896.
- Baydogan, M. G., Runger, G. and Tuv, E. (2013), ‘A bag-of-features framework to classify time series’, *IEEE transactions on pattern analysis and machine intelligence* **35**(11), 2796–2802.
- Chen, T. and Guestrin, C. (2016), Xgboost:a scalable tree boosting system, in ‘ACM SIGKDD International Conference on Knowledge Discovery and Data Mining’, pp. 785–794.
- Collopy, F. and Armstrong, J. S. (1992), ‘Rule-based forecasting: development and validation of an expert systems approach to combining time series extrapolations’, *Management Science* **38**(10), 1394–1414.
- Deng, J., Dong, W., Socher, R., Li, L. J., Li, K. and Li, F. F. (2009), Imagenet: A large-scale hierarchical image database, in ‘IEEE Conference on Computer Vision and Pattern Recognition’.

- Donahue, J., Jia, Y., Vinyals, O., Hoffman, J., Ning, Z., Tzeng, E., Darrell, T., Donahue, J., Jia, Y. and Vinyals, O. (2014), Decaf: A deep convolutional activation feature for generic visual recognition, in ‘International Conference on International Conference on Machine Learning’.
- Eckmann, J.-P., Kamphorst, S. O. and Ruelle, D. (1987), ‘Recurrence plots of dynamical systems’, *EPL (Europhysics Letters)* **4**(9), 973.
- Fulcher, B. D. (2018), Feature-based time-series analysis, in ‘Feature engineering for machine learning and data analytics’, CRC Press, pp. 87–116.
- Fulcher, B. D., Little, M. A. and Jones, N. S. (2013), ‘Highly comparative time-series analysis: the empirical structure of time series and their methods’, *Journal of the Royal Society Interface* **10**(83), 20130048.
- Fulcher, B. and Jones, N. (2014), ‘Highly comparative feature-based time-series classification’, *IEEE Transactions on Knowledge and Data Engineering* **26**(12), 3026–3037.
- Ge, W. and Yu, Y. (2017), Borrowing treasures from the wealthy: Deep transfer learning through selective joint fine-tuning, in ‘Computer Vision and Pattern Recognition’.
- Han, D., Liu, Q. and Fan, W. (2018), ‘A new image classification method using cnn transfer learning and web data augmentation’, *Expert Systems With Applications* **95**, 43–56.
- Hatami, N., Gavet, Y. and Debayle, J. (2017), ‘Bag of recurrence patterns representation for time-series classification’, *Pattern Analysis and Applications* pp. 1–11.
- He, K., Zhang, X., Ren, S. and Sun, J. (2016), Deep residual learning for image recognition, in ‘Proceedings of the IEEE conference on computer vision and pattern recognition’, pp. 770–778.
- Hyndman, R. J., Wang, E. and Laptev, N. (2015), Large-scale unusual time series detection, in ‘Proceedings of the IEEE International Conference on Data Mining’, Atlantic City, NJ, USA. 14–17 November 2015.
- Kang, Y., Hyndman, R. J. and Smith-Miles, K. (2017), ‘Visualising forecasting algorithm performance using time series instance spaces’, *International Journal of Forecasting* **33**(2), 345–358.
- Krizhevsky, A., Sutskever, I. and E. Hinton, G. (2012), ‘Imagenet classification with deep convolutional neural networks’, *Neural Information Processing Systems* **25**.
- Lazebnik, S., Schmid, C. and Ponce, J. (2006), Beyond bags of features: Spatial pyramid matching for recognizing natural scene categories, in ‘2006 IEEE Computer Society Conference on Computer Vision and Pattern Recognition (CVPR’06)’, Vol. 2, IEEE, pp. 2169–2178.
- Lowe, D. G. (1999), Object recognition from local scale-invariant features, in ‘Computer vision, 1999. The proceedings of the seventh IEEE international conference on’, Vol. 2, IEEE, pp. 1150–1157.

- Maaten, L. v. d. (2014), ‘Accelerating t-SNE using tree-based algorithms’, *The Journal of Machine Learning Research* **15**(1), 3221–3245.
- Makridakis, S. and Hibon, M. (2000), ‘The M3-Competition: results, conclusions and implications’, *International Journal of Forecasting* **16**(4), 451–476.
- Makridakis, S., Spiliotis, E. and Assimakopoulos, V. (2018), ‘The m4 competition: Results, findings, conclusion and way forward’, *International Journal of Forecasting* **34**(4), 802–808.
- Meade, N. (2000), ‘Evidence for the selection of forecasting methods’, *Journal of Forecasting* **19**(6), 515–535.
- Montero-Manso, P., Athanasopoulos, G., Hyndman, R. J. and Talagala, T. S. (2020), ‘FFORMA: Feature-based forecast model averaging’, *International Journal of Forecasting* **36**(1), 86 – 92.
- Nanopoulos, A., Alcock, R. and Manolopoulos, Y. (2001), ‘Feature-based classification of time-series data’, *International Journal of Computer Research* **10**(3).
- Pan, S. J. and Qiang, Y. (2010), ‘A survey on transfer learning’, *IEEE Transactions on Knowledge and Data Engineering* **22**(10), 1345–1359.
- Petropoulos, F., Makridakis, S., Assimakopoulos, V. and Nikolopoulos, K. (2014), ‘Horses for courses’ in demand forecasting’, *European Journal of Operational Research* **237**(1), 152–163.
- Razavian, A. S., Azizpour, H., Sullivan, J. and Carlsson, S. (2014), ‘Cnn features off-the-shelf: An astounding baseline for recognition’.
- Shah, C. (1997), ‘Model selection in univariate time series forecasting using discriminant analysis’, *International Journal of Forecasting* **13**(4), 489–500.
- Simonyan, K. and Zisserman, A. (2014), ‘Very deep convolutional networks for large-scale image recognition’, *Computer Science* .
- Szegedy, C., Liu, W., Jia, Y., Sermanet, P., Reed, S., Anguelov, D., Erhan, D., Vanhoucke, V. and Rabinovich, A. (2015), Going deeper with convolutions, in ‘Proceedings of the IEEE conference on computer vision and pattern recognition’, pp. 1–9.
- Talagala, P. D., Hyndman, R. J., Smith-Miles, K., Kandanaarachchi, S. and Muñoz, M. A. (2019), ‘Anomaly detection in streaming nonstationary temporal data’, *Journal of Computational and Graphical Statistics* (In press), 1–28.
- Talagala, T. S., Hyndman, R. J. and Athanasopoulos, G. (2018), Meta-learning how to forecast time series, Working paper 6/18, Monash University, Department of Econometrics and Business Statistics.
- Thiel, M., Romano, M. C. and Kurths, J. (2004), ‘How much information is contained in a recurrence plot?’, *Physics Letters A* **330**(5), 343–349.

- Wang, J., Liu, P., She, M. F., Nahavandi, S. and Kouzani, A. (2013), ‘Bag-of-words representation for biomedical time series classification’, *Biomedical Signal Processing and Control* **8**(6), 634–644.
- Wang, J., Yang, J., Yu, K., Lv, F., Huang, T. and Gong, Y. (2010), Locality-constrained linear coding for image classification, *in* ‘Computer Vision and Pattern Recognition (CVPR), 2010 IEEE Conference on’, IEEE, pp. 3360–3367.
- Wang, X., Smith, K. A. and Hyndman, R. J. (2006), ‘Characteristic-based clustering for time series data’, *Data Mining and Knowledge Discovery* **13**(3), 335–364.
- Wang, X., Smith-Miles, K. A. and Hyndman, R. J. (2009), ‘Rule induction for forecasting method selection: meta-learning the characteristics of univariate time series’, *Neurocomputing* **72**(10-12), 2581–2594.
- Wang, Z. and Oates, T. (2015), Imaging time-series to improve classification and imputation, *in* ‘Proceedings of the 24th International Conference on Artificial Intelligence’, AAAI Press, pp. 3939–3945.

Appendix

Experimental setup

In the traditional image processing method SIFT, before linear coding, we need to obtain the basic descriptors; $k = 200$ is chosen as the number of clusters. 200 centroid coordinates are used as the coordinates of basic descriptors. We select 5 close descriptors from 200 basic descriptors for each descriptor with the K-nearest neighbors (KNN) algorithm and the adjustment factor $\lambda = e^{-4}$ in LLC. We choose 1, 2 and 4 as the SPM parameters. We split the image by 1×1 , 2×2 and 4×4 , respectively.

The parameters for the recurrence plot are set as follows:

- Parameter of eps: 0.1.
- Parameter of steps: 5.

The parameters for SIFT are set as follows:

- Number of basic descriptors: 200. Basic descriptors are obtained with k-means clustering.
- LLC Parameter: $k = 5$ in KNN. The adjustment factor $\lambda = e^{-4}$.
- SPM Parameter: 1, 2 and 4. We split the images by 1×1 , 2×2 and 4×4 .
- Number of extracted features from each image: $200 \times (1 \times 1 + 2 \times 2 + 4 \times 4) = 4200$.

The parameters for the pretrained CNN models are set as follows:

- Dimension of the output of the pretrained Inception-v1 model: 1024.
- Dimension of the output of the pretrained ResNet-v1-101 model: 2048.
- Dimension of the output of the pretrained ResNet-v1-50 model: 2048.
- Dimension of the output of the pretrained VGG model: 1000.

In model averaging, we need to set parameters for XGBoost. We performed a search in a subset of the hyperparameter spaces, measuring the OWA via 10-fold cross-validation of the training data.

The hyperparameters are set as follows:

- The maximum depth of a tree ranges from 6 to 50.
- The learning rate and the scale of contribution of each tree ranges from 0.001 to 1.
- The proportion of the training set used to calculate the trees in each iteration ranges from 0.5 to 1.
- The proportion of features used to calculate the trees in each iteration ranges from 0.5 to 1.
- The number of iterations of the algorithm ranges from 1 to 250.